telecom

MDPI

Article

Error Performance Estimation of Modulated Retroreflective Transdermal Optical Wireless Links with Diversity under Generalized Pointing Errors

George K. Varotsos [1], Hector E. Nistazakis [1,*], Konstantinos Aidinis [2], Fadi Jaber [3], Mohd Nasor [3] and Kanhira Kadavath Mujeeb Rahman [3]

[1] Section of Electronic Physics and Systems, Department of Physics, National and Kapodistrian University of Athens, 15784 Athens, Greece; georgevar@phys.uoa.gr
[2] Department of Electrical and Computer Engineering, Ajman University, Ajman P.O. Box 346, United Arab Emirates; k.aidinis@ajman.ac.ae
[3] Department of Biomedical Engineering, Ajman University, Ajman P.O. Box 346, United Arab Emirates; f.jaber@ajman.ac.ae (F.J.); m.nasor@ajman.ac.ae (M.N.); m.rahman@ajman.ac.ae (K.K.M.R.)
* Correspondence: enistaz@phys.uoa.gr; Tel.: +30-210-7276710

Abstract: Recent developments in both optical wireless communication (OWC) systems and implanted medical devices (IMDs) have introduced transdermal optical wireless (TOW) technology as a viable candidate for extremely high-speed in-body to out-of-body wireless data transmissions, which are growing in demand for many vital biomedical applications, including telemetry with medical implants, health monitoring, neural recording and prostheses. Nevertheless, this emerging communication modality is primarily hindered by skin-induced attenuation of the propagating signal bit carrier along with its stochastic misalignment-induced fading. Thus, by considering a typical modulated retroreflective (MRR) TOW system with spatial diversity and optimal combining (OC) for signal reception in this work, we focus, for the first time in the MRR TOW literature, on the stochastic nature of generalized pointing errors with non-zero boresight (NZB). Specifically, under these circumstances, novel analytical mathematical expressions were derived for the total average bit error rate (BER) of various system configurations. Their results revealed significant outage performance enhancements when spatial diversity was utilized. Moreover, taking into consideration the total transdermal pathloss along with the effects of stochastic NZB pointing errors, the critical average signal-to-noise ratio (SNR) metric was evaluated for typical power spectral-density values.

Keywords: optical wireless communications; implanted medical devices; transdermal optical wireless communication; modulated retroreflective link; pointing errors with nonzero boresight; transdermal pathloss; diversity; average bit error rate; optimal combining

Citation: Varotsos, G.K.; Nistazakis, H.E.; Aidinis, K.; Jaber, F.; Nasor, M.; Rahman, K.K.M. Error Performance Estimation of Modulated Retroreflective Transdermal Optical Wireless Links with Diversity under Generalized Pointing Errors. *Telecom* **2021**, *2*, 167–180. https://doi.org/10.3390/telecom2020011

Academic Editor: Sotirios Goudos

Received: 31 December 2020
Accepted: 29 March 2021
Published: 1 April 2021

1. Introduction

Transdermal optical wireless links that transmit information data via light waves through the skin have lately attracted particular research and commercial interest, mainly due to their effective high-speed operation within a very large unlicensed available bandwidth with low probability of intercept, low power consumption, ease of modulation and demodulation, compact and light equipment, flexibility for deployment and redeployment, and electromagnetic interference (EMI) immunity, [1–6]. In view of these concrete advantages over their radio frequency (RF) and inductive-coupling counterparts, which are widely used in most transcutaneous communication systems with medical implants nowadays, TOW (transdermal optical wireless) technology affords a prime alternative, if not the only viable choice for establishing robust transdermal wireless communication links that can simultaneously reach the growing high capacity and low power requirements of different but equally important medical applications such as natural-feeling prosthetic

control, neural cortical signal recording and communication with cochlear implants, as revealed in the findings of [7–11].

However, since skin is a very complex, multilayered and optically turbid channel that consists of many different structural components, the information-bearing light that propagates through the skin is reflected, scattered and absorbed by all these skin structural components, [10,12–14]. In fact, even within the medical optical window; i.e., the desirable wavelength regime between 0.6μm and 1.3μm where photon absorption by tissue is minimized, skin highly attenuates the information-bearing light signal and limits its maximum depth of penetration into tissue by as much as several centimeters, [1,7,8,14–16].

Apart from transdermal pathloss, TOW performance and availability is strongly degraded by the effect of pointing errors due to random misalignments between transmitter and receiver apertures that result, in turn, in significant random misalignment-induced irradiance fading of the propagating information-bearing light signal at the receiver side, [17,18]. Indeed, despite the directional behavior of light sources and photodetectors, the relative motion between the transmitter and receiver in several biomedical applications is unavoidable due to biological functions [19]. Thus, in such cases the stochastic nature of pointing errors should not be neglected. More specifically, however, pointing errors consist of two components: boresight and jitter. The former represents the fixed displacement between the beam and the detector center, and the latter is the random offset of the beam center at the detector plane [12,20,21].

Hence, as is the case with the spatial-diversity technique, in which single-input multiple-output (SIMO) link configurations are employed, it could be more realistic to also consider boresight, i.e., NZB (non-zero boresight) pointing errors (PEs), since the transmitted light beam can be strictly aligned with only one photodetector due to the fixed spacing among the receiver apertures. It is to be recalled here that diversity is realized usually, in space, in time or in wavelength, and refers to the consideration of multiple copies of the propagated signals in an attempt to overcome a poor transmission media state [17,20–22]. Consequently, through spatial diversity, the system can incorporate multiple receiver apertures [5].

At this point, we should clarify that there are two basic TOW link configurations: direct and MRR (modulated retroreflective) [3,4,23]. Through the former, the modulated light traverses the cutaneous channel in order to be collected at the receiver side, while through the latter, the in-body MRR modulates the transmitted interrogating light beam and reflects it back to the out-of-body receiver terminal. Consequently, since the light signal passes through the skin channel twice, the impact of the skin-induced attenuation effect becomes more significant in the latter case. However, the latter configuration has the distinct advantage of placing both transmitter and receiver terminals on the outside of body, which makes this configuration much more flexible for deployment and redeployment [18,23]. Additionally, it makes possible to conserve the energy of the battery of the implanted device in a more effective and flexible way [3,18].

It is noteworthy that the feasibility of both direct and MRR TOW link modalities have been experimentally validated in [1,7,8,10,13,15] and in [1,3], respectively. Nevertheless, in all these papers, the effect of pointing errors has been either neglected or described by deterministic models. The stochastic nature of zero-boresight pointing errors for direct TOW links has been only recently first modeled and quantified by the authors in [11,19,24,25]. Next, the authors in [12,17] extended this concept by modeling the more generalized NZB pointing errors impact on direct TOW typical links with diversity in space, in time or in wavelength. More recently, the authors in [4,18] introduced the presence of stochastic zero-boresight pointing errors for MRR TOW links with diversity. In particular, the total outage probability and the total average bit error rate (ABER) have been evaluated in [18] and in [4], respectively.

Thus, to the best of our knowledge, the influence of NZB pointing errors has not yet been estimated for MRR TOW links with diversity. Moreover, contrary to the research that has been conducted for direct TOW links, there are still only a few papers that reported on MRR TOW links. Motivated by these facts, in this work, we introduce the presence

of stochastic NZB pointing errors for MRR TOW links with spatial diversity, along with the OC (optimal combining) technique for signal reception. The total error performance of the investigated system is evaluated through the critical ABER performance metric. Specifically, an ABER analysis is performed that includes the most crucial link parameters, such as the skin thickness, the transdermal pathloss and the intensity of PE with NZB. In this context, the joint impact of spatial diversity, along with NZB stochastic pointing errors, is assessed and quantified. Indeed, novel ABER expressions are derived that mainly incorporate the number of the utilized receiver apertures, the total transdermal distance and the NZB pointing errors' strength. Additionally, representative analytical ABER results are presented over a wide average electrical SNR (signal-to-noise ratio) range and are further validated by simulations. Furthermore, in order to verify the feasibility of achieving such average SNR values, i.e., without exceeding the maximum power levels permitted for transdermal links with IMDs (implanted medical devices), we estimate the average electrical SNR obtained for appropriate power spectral (PSD) density values, taking into account the total transdermal pathloss together with the NZB pointing errors' strength for each MMR TOW link.

In short, the main contributions of this paper can be summarized as follows:

- A novel system and channel model for MRR TOW links is developed that incorporates the basic characteristics of this type of link.
- The impact of the more realistic stochastic pointing errors with nonzero boresight is introduced and estimated in the MRR TOW area for the first time.
- A spatial-diversity technique with optimal combining is considered by employing multiple out-of-body receiver apertures, and thus, MRR TOW data transmissions of enhanced reliability are achieved.
- An outage bit error rate analysis is performed that evaluates the effectiveness of the spatial-diversity technique versus the joint impact of transdermal pathloss and generalized pointing errors with nonzero boresight.
- An average SNR estimation is performed that reveals the feasibility of the proposed MRR TOW system architecture.
- Novel analytical mathematical expressions are derived along with proper corresponding illustrated results that can be utilized in the design of MRR TOW links.

2. System and Channel Model

2.1. Signal Model

The out-of-body transmitter terminal is assumed to employ just one laser source, while the receiver terminal, which is also assumed to be placed on the outside of the body, comprises $m = 1, 2, ..., M$ different, spatially separated detector apertures, i.e., see Figure 1.

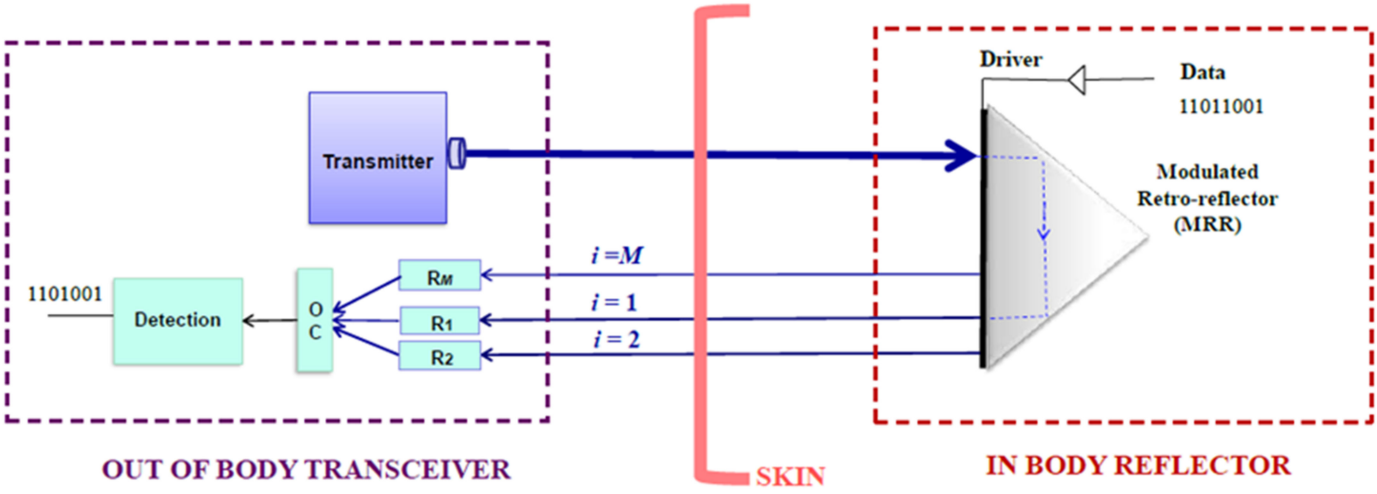

Figure 1. Block diagram of the proposed MRR TOW system.

Apart from the IMD, the only part of the investigated TOW communication system that is needed to be installed inside the body is the retromodulator with its drive electronics. Initially, the laser source emits an interrogating light beam, which propagates through the skin and illuminates the internal retroreflector. The latter modulates the incoming light beam with on-off keying (OOK) and reflects it back to the receiver terminal. Consequently, the reflected light is modulated to reflect the information data to be transmitted. When the information-bearing light arrives at the receiver terminal, it is collected by its receiver aperture(s). At this point, by also using the OC technique, the intensity of the light signal is directly detected and demodulated in an attempt to recover the information data. It is worth mentioning that so far, OOK with intensity modulation and direct detection IM/DD is the only modulation format that has been practically utilized in both direct and MRR TOW link configurations, [1,3,7–10], mainly because it outperforms in terms of simplicity, compactness and lightweight device equipment, which is very critical for any transdermal communication link design and feasibility. Nevertheless, when OOK is operating under fading conditions, the detector threshold must be estimated and adjusted by appropriate means, according to the variable skin channel states [12]. Therefore, perfect skin channel state information (CSI) needs to be assumed in order to perform optimal signal detection. In this context, the statistical skin channel model can be roughly expressed as [4,5,18,25]:

$$y_m = \eta_m h_m x + n \tag{1}$$

where y_m represents the m-th signal copy arriving at the m-th receiver's aperture with m = 1, 2, ..., M; η_m is the corresponding effective photodiode's photo-current conversion ratio; x is the information bit signal; h_m denotes the m-th total channel state; and n is the additive noise that is modeled as a zero-mean complex Gaussian process with variance σ^2 [5,12,25].

Each total skin channel state h_m can be obtained as $h_m = h_{T,m}h_{R,m} = h_{T,l,m}h_{R,l,m}h_{p,m}$, where $h_{T,m}$ and $h_{R,m}$ represent the m-th channel state for the m-th forward-interrogating and backward-retroreflected path, respectively, [4,18,26]. Additionally, $h_{T,l,m}$ and $h_{R,l,m}$ stand for the deterministic channel coefficients due to the corresponding transdermal pathloss, while $h_{p,m}$ refers to the corresponding stochastic process that models the misalignment-induced geometric spreading [5,11,12,24–30]. Therefore, $h_{T,m} = h_{T,l,m}$, and $h_{R,m} = h_{R,l,m}h_{p,m}$, while by assuming without loss of generality that $h_{T,l,m} = h_{R,l,m} = h_{l,m}$, the total m-th channel state can be expressed as [4,18]:

$$h_m = h_{l,m}^2 h_{p,m}, \tag{2}$$

Each transdermal pathloss component $h_{l,m}$ can be obtained as:

$$h_{l,m} = \exp\left[-\frac{1}{2}\alpha(\lambda_m)\delta_m\right], \tag{3}$$

where δ_m is the dermal thickness of the m-th transmitted or reflected transdermal path, and $\alpha(\lambda_m)$ is its skin-attenuation coefficient, with λ_m being the corresponding operational wavelength. For operational wavelengths between 400 nm and 1800 nm, we obtain [11,24,25]:

$$\alpha(\lambda_m) = \sum_{i=1}^{8} a_i \exp\left[-\left(\frac{\lambda_m - b_i}{c_i}\right)^2\right], \tag{4}$$

where λ_m values are expressed in nm and the values of a_i, b_i and c_i, with i = 1, 2, ...,8, are obtained from ([19], Table 1). It is noteworthy that the accuracy of the latter expression is higher than 99.7% [19,25].

Table 1. Parameter a_i, b_i and c_i values [19].

i	a_i	b_i	c_i
1	10	0.35	0.065
2	4.5	0.42	0.25
3	13.48	−1.5	50.12
4	14.7	1442	49.35
5	7.435	1499	75.88
6	48	3322	1033
7	594.1	−183	285.9
8	11.47	−618.5	1054

2.2. Generalized Pointing Errors with Nonzero Boresight

Apart from beam width and photodetector(s) size, which have been considered through the well-known zero-boresight pointing error model, first introduced in [27] for free-air communications and in [24] for TOW links, we also take into account the NZB along with nonidentical jitters for the elevation and the horizontal displacement. Consequently, since the Gaussian light beam traverses each backward transdermal path of δ_m in length, the corresponding fraction of the collected power at the m-th receiver circular aperture with radius r_m, can be approximated as [12,27]:

$$h_{p,m}(R_m, \delta_m) \approx A_{0,m} \exp\left(-\frac{2R_m^2}{w_{eq,m}^2}\right), \; R_m \geq 0, \tag{5}$$

where $w_{eq,m}$ represents the equivalent beam width in the m-th receiver aperture, which is given as $w_{eq,m} = \left[\frac{\sqrt{\pi}\text{erf}(v_m)w_{\delta,m}^2}{2v_m \exp(-v_m^2)}\right]^{1/2}$, with $v_m = \frac{\sqrt{\pi}r_m}{\sqrt{2}w_{\delta,m}}$ and erf(.) denoting the error function ([31], Equation (8.250.1)). Additionally, in TOW links we get [6,11,18]:

$$w_{\delta,m} = \delta_m \tan(\theta_m/2) \tag{6}$$

where $w_{\delta,m}$ represents the m-th beam waist on the receiver(s) plane at distance δ_m from the implanted retroreflective modulator, with θ_m being the corresponding divergence angle [4,25]. Moreover, $A_{0,m} = \text{erf}^2(v_m)$ is the fraction of the collected power at r_m=0, [5,17]. Furthermore, R_m is the radial displacement at the m-th receiver, which is expressed as $R_m = \left|\vec{R}_m\right| = \sqrt{R_{x,m}^2 + R_{y,m}^2}$, where $\vec{R}_m = \left[R_{x,m}, R_{y,m}\right]^T$ is the radial displacement vector with $R_{x,m}$, $R_{y,m}$ being the displacements located along the horizontal and elevation axes at the detector plane, respectively. It should be noted that these variables are considered as nonzero mean Gaussian distributed random variables, i.e., $R_{x,m} \sim N\left(\mu_{x,m}, \sigma_{x,m}^2\right)$, $R_{y,m} \sim N\left(\mu_{y,m}, \sigma_{y,m}^2\right)$, where $\mu_{x,m}$, $\mu_{y,m}$, denote their mean values and $\sigma_{x,m}$, $\sigma_{y,m}$ are the jitters for horizontal and elevation displacements, respectively, [12,28]. Here, it should be also mentioned that the approximation of Equation (5) is valid for $w_{\delta,m}/\, r_m > 6$, which is true in typical optical wireless links, [27,28,30].

Considering thus the beam width, the photodetector size(s) and the different jitter for the elevation and horizontal displacements, along with NZB, the misalignment-induced irradiance fading at each receiver aperture can be described by the suitable generalized Beckmann's distribution model [32]:

$$f_{R,m}(R_m) = \frac{R_m}{2\pi\sigma_{x,m}\sigma_{y,m}} \times \int_0^{2\pi} \exp\left[-\frac{(R_m\cos\varphi_m - \mu_{x,m})^2}{2\sigma_{x,m}^2} - \frac{\left(R\sin\varphi_m - \mu_y\right)^2}{2\sigma_y^2}\right] d\varphi_m \tag{7}$$

where φ_m is the m-th reflected divergence angle, which stands for the increase in beam radius with distance from the modulated retroreflector [17].

It has been first shown in [30] that the Beckmann's distribution above can be approximated according to the modified Rayleigh distribution:

$$f_{R,m}(R_m) = \frac{R_m}{\sigma^2_{\text{mod},m}} \exp\left(-\frac{R_m^2}{2\sigma^2_{\text{mod},m}}\right), \; R_m \geq 0, \tag{8}$$

where $\sigma^2_{\text{mod},m} = \left(\frac{3\mu^2_{x,m}\sigma^4_{x,m}+3\mu^2_{y,m}\sigma^4_{y,m}+\sigma^6_{x,m}+\sigma^6_{y,m}}{2}\right)^{\frac{1}{3}}$, with $\sigma_{mod,m}$ being the joint modified jitter (standard deviation) of $\sigma_{x,m}$ and $\sigma_{y,m}$ for the m-th reflected transdermal path, [12,21,30].

In view of the above, the probability density function (PDF) of the random variable $h_{p,m}$ is given as [4,19]:

$$f_{h_{p,m}}(h_{p,m}) = \xi_m^2 (A_{0,m} g_m)^{-\xi_m^2} h_{p,m}^{\xi_m^2 - 1}, \quad 0 \leq h_{p,m} \leq g_m A_{0,m}, \tag{9}$$

where the parameter g_m is obtained as [17,28,29]:

$$g_m = \exp\left(\frac{1}{\xi_m^2} - \frac{1}{2\xi_{x,m}^2} - \frac{1}{2\xi_{y,m}^2} - \frac{\mu_{x,m}^2}{2\sigma_{x,m}^2\xi_{x,m}^2} - \frac{\mu_{y,m}^2}{2\sigma_{y,m}^2\xi_{y,m}^2}\right), \tag{10}$$

with $\xi_m = \frac{w_{eq,m}}{2\sigma_{mod,m}}$, $\xi_{x,m} = \frac{w_{eq,m}}{2\sigma_{x,m}}$, $\xi_{y,m} = \frac{w_{eq,m}}{2\sigma_{y,m}}$ describing the corresponding misalignment-induced fading strength. In fact, the pointing-error effect becomes more significant for lower values of ξ_m. Therefore, for very large values of ξ_m,the effect of pointing errors can be considered as a negligible one, [12,20]. Additionally, it should be noted that considering $\mu^2_{x,m} = \mu^2_{y,m} = 0$, $\sigma^2_{x,m} = \sigma^2_{y,m} = \sigma_s^2$ and $g_m = 1$, the PDF including NZB boresight in Equation (9) reduces to the well-known one for zero-boresight pointing errors presented first in ([27], Equation (11)).

2.3. Joint Impact of Pathloss and Generalized Pointing Errors with Nonzero Boresight

By using Equations (2), (3) and (9) and applying a random variable (RV) transformation [33], the joint PDF of the random variable hh_m is obtained as:

$$f_{h_m}(h_m) = \xi_m^2 (A_{0,m} g_m)^{-\xi_m^2} h_{l,m}^{-2\xi_m^2} h_m^{\xi_m^2 - 1}, \; 0 \leq h_m \leq A_{0,m} g_m h_{l,m}, \tag{11}$$

Furthermore, taking into consideration Equations (1)–(3), the instantaneous electrical SNR, γ_m, can be obtained as:

$$\gamma_m = \frac{\eta_m^2 h_m^2 P_s}{N_0} = \frac{\eta_m^2 h_{l,m}^4 h_{p,m}^2 P_s}{N_0}, \tag{12}$$

where P_s and N_0 stand for the signal and noise optical PSD, respectively, [25].

Thus, by considering Equation (12), the average electrical SNR, $\rho_m = E[\gamma_m]$, is obtained as [19]:

$$\rho_m = \frac{\eta_m^2 E^2[h_m] P_S}{N_0} = \frac{\eta_m^2 \xi_m^2 A_{0,m}^2 g_m^2 h_{l,m}^4 P_S}{(\xi_m^2 + 2) N_0}. \tag{13}$$

2.4. SISO MRR TOW Links

Assuming OOK with intensity modulation and direct detection (IM/DD), the instantaneous BER (bit error rate) for each examined TOW backward link is given as [20]:

$$P_e(h_m) = \frac{1}{2} erfc\left(\eta_m h_m / 2\sqrt{N_0}\right), \tag{14}$$

where *erfc*(.) denotes the complementary error function ([31], Equation (8.250.4)). By averaging Equation (14) over h_m, the ABER, $P_{e,av}$, is expressed as [22]:

$$P_{e,av} = \int_0^\infty P_e(h_m) f_{h_m}(h_m) dh_m. \tag{15}$$

By substituting Equations (11) and (14) into Equation (15) and by then using $\int_0^\infty t^{z-1} erfc(t) dt = \frac{1}{\sqrt{\pi} z} \Gamma\left(\frac{z+1}{2}\right)$, $Re(z) > 0$ ([34], Equation (06.27.21.0132.01)), the corresponding ABER is obtained as:

$$P_{e,av} = \left(2\sqrt{\pi} A_{0,m}^{\xi_m^2} g_m^{\xi_m^2}\right)^{-1} h_{l,m}^{-2\xi_m^2} \left(2\sqrt{N_0}/\eta_m\right)^{\xi_m^2} \Gamma\left[\left(\xi_m^2 + 1\right)/2\right], \tag{16}$$

where Γ(.) stands for the gamma function ([34], Equation (06.05.02.0001.01)).

2.5. SIMO MRR TOW Links with Spatial Diversity and OC

The total ABER metric for the investigated TOW MRR system with spatial diversity and OC signal reception is given as [4,12,22]:

$$P_{e,av,M}^{OC} = \int_{\vec{h}} f_{\vec{h}}\left(\vec{h}\right) Q\left(\frac{1}{\sqrt{2MN_0}} \sqrt{\sum_{m=1}^{M} (\eta_m h_m)^2}\right) d\vec{h}, \tag{17}$$

where $\vec{h} = [h_1, h_2, \ldots, h_M]$ is the vector of the total channel state for each one of the M copies of the propagating light signal.

By substituting the accurate approximation of [35] for the Q-function, i.e., $Q \approx \frac{1}{12}\left[exp\left(\frac{-x^2}{2}\right) + 3exp\left(\frac{-2x^2}{3}\right)\right]$, into Equation (17), the latter expression gives [36]:

$$P_{e,av,M}^{OC} \approx \frac{1}{12} \prod_{m=1}^{M} \int_0^\infty \exp\left(-\frac{\eta_m^2 h_m^2}{4MN_0}\right) f_{h_m}(h_m) dh_m + \frac{1}{4} \prod_{m=1}^{M} \int_0^\infty \exp\left(-\frac{\eta_m^2 h_m^2}{3MN_0}\right) f_{h_m}(h_m) dh_m. \tag{18}$$

By utilizing for each integral above $\int_0^\infty x^n exp(-zx^2) dx = \frac{\Gamma\left(\frac{n+1}{2}\right)}{2z^{\frac{(n+1)}{2}}}$, $n > -1$, $Re(z) > 0$ ([34] Equation (06.05.02.0001.01)), and by then using Equation (13), we conclude with the following analytical total ABER expression for the examined IM/DD OOK MRR TOW system with spatial diversity, NZB stochastic pointing errors and OC reception technique for the signal:

$$\begin{aligned} P_{e,av,M}^{OC} \approx & \frac{1}{12} \prod_{m=1}^{M} \frac{\xi_m \left[\rho_m \left(\xi_m^2 + 2\right)\right]^{-\xi_m^2/2} \Gamma\left(\xi_m^2/2\right)}{2(4M)^{-\xi_m^2/2}} \\ & + \frac{1}{4} \prod_{m=1}^{M} \frac{\xi_m \left[\rho_m \left(\xi_m^2 + 2\right)\right]^{-\xi_m^2/2} \Gamma\left(\xi_m^2/2\right)}{2(3M)^{-\xi_m^2/2}} \end{aligned} \tag{19}$$

3. Analytical Results

In this section, we initially present the ABER performance outcomes obtained by the analytical expressions extracted; i.e., Equations (16) and (19), through the mathematical analysis performed above. Most of them were verified by simulations in order to highlight the accuracy of the derived expressions and the analysis proposed. In this context, by assuming weak to strong NZB pointing errors along with transdermal pathloss, the beneficial impact of spatial diversity on ABER performance enhancement, with OC technique, was revealed. Next, the power efficiency of the proposed MRR TOW system was evaluated in terms of its attainable average electrical SNR within a specific and desirable power-density-spectrum regime, considering once again transdermal pathloss and stochastic NZB pointing errors. In this context, the derived average SNR expression in Equation (12) was

utilized. The representative results demonstrated the feasibility of the proposed MRR TOW links in terms of this important metric.

In view of the above, we made the assumptions below and we adopted the following parameter values, i.e., see Table 2. The investigated MRR TOW system could employ from one to three photodetector apertures, i.e., $M = \{1, 2, 3\}$. Consequently, for $M = 1$, we obtained a SISO MRR TOW link without diversity, while when $M > 1$, the spatial-diversity technique was utilized and thus, SIMO MRR TOW links were created. Note that for the former SISO link configuration, we addressed only zero-boresight pointing errors, while for the latter SIMO link configurations, pointing errors with NZB also appeared and must be taken into account. For each forward or backward transdermal link, the skin thickness, δ_m, was assumed to be equal to 7 mm or 8 mm, while the divergence angle, θ_m, was set to 20°. Furthermore, unless otherwise stated, it was assumed that P_s = 1 μw/MHz, while N_0 is fixed at $\left(1.3\,\text{pA}/\sqrt{\text{Hz}}\right)^2$ [37]. Additionally, for each TOW link, the operational wavelength, λ_m, was selected to be equal to 1.1μm, since according to [19], this is the optimal transmission wavelength value for TOW links. It became evident that the choice of the appropriate operational wavelength was even more critical for MRR TOW links, where the light signal traverses the skin channel twice, which makes it even more susceptible to skin-induced attenuation and transdermal pathloss. Regarding pointing errors, considering the above parameter values, we obtained $w_{\delta,m}/r_m > 6$, which made the approximation in Equation (5) valid. Additionally, for $M = 1$, we assumed zero-boresight pointing errors either with $(\delta_m, \mu_{x,m}/r_m,\ \mu_{y,m}/r_m,\ \sigma_{x,m}/r_m,\ \sigma_{y,m}/r_m) = (7\,\text{mm}, 0, 0, 4, 4)$; i.e., $\xi_1 = 1.14$; or $(\delta_m, \mu_{x,m}/r_m,\ \mu_{y,m}/r_m,\ \sigma_{x,m}/r_m,\ \sigma_{y,m}/r_m) = (8\,\text{mm}, 0, 0, 4, 4)$; i.e., $\xi_1 = 1.30$. For $M = 2$, we also assumed NZB pointing errors for the second photodetector with $(\delta_m, \mu_{x,m}/r_m,\ \mu_{y,m}/r_m,\ \sigma_{x,m}/r_m,\ \sigma_{y,m}/r_m) = (7\,\text{mm}, 2, 1, 4.5, 4.5)$; i.e., $\xi_2 = 0.96$; $(\delta_m, \mu_{x,m}/r_m,\ \mu_{y,m}/r_m,\ \sigma_{x,m}/r_m,\ \sigma_{y,m}/r_m) = (7\,\text{mm}, 2, 1, 5, 5)$; i.e., $\xi_2 = 0.99$; $(\delta_m, \mu_{x,m}/r_m,\ \mu_{y,m}/r_m,\ \sigma_{x,m}/r_m,\ \sigma_{y,m}/r_m) = (8\,\text{mm}, 2, 1, 4.5, 4.5)$; i.e., $\xi_2 = 0.87$; and $(\delta_m, \mu_{x,m}/r_m,\ \mu_{y,m}/r_m,\ \sigma_{x,m}/r_m,\ \sigma_{y,m}/r_m) = (8\,\text{mm}, 2, 1, 5, 5)$; i.e., $\xi_2 = 1.10$. Finally, for $M = 3$, we correspondingly assumed $\xi_2 = \xi_3 = 0.96$, 0.99, 0.87 or 1.10. Under these assumptions and settings, the following analytical and simulation results are presented.

Table 2. Link parameter values.

Parameter	Value(s)
θ_m	20°
P_s	1 μW/MHz–20 μW/MHz
N_0	$\left(1.3\,\text{pA}/\sqrt{\text{Hz}}\right)^2$
μ	30–60 dB
η_m	0.8
M	{1, 2, 3}
λ_m	1.1 μm
r_m	0.5 mm
δ_m	{7 mm, 8 mm}
$\mu_{x,m}/\ r_m$	{0, 2}
$\mu_{y,m}/\ r_m$	{0, 1}
$\sigma_{x,m}/\ r_m$	{4, 4.5, 5}
$\sigma_{y,m}/\ r_m$	{4, 4.5, 5}
ξ_1	{1.14, 1.30}
ξ_2	{0.87, 0.96, 0.99, 1.10}
ξ_3	{0.87, 0.96, 0.99, 1.10}

Figure 2 shows the ABER evolution of the examined MRR TOW system over a wide average electrical SNR range for both SISO and SIMO configurations with OC, assuming different levels of stochastic pointing mismatch. The skin thickness was fixed at 7 mm. In any case, the illustrated results indicated that the total ABER decreased for larger average electrical SNR values. Indeed, lower ABER values needed higher electrical SNR values

to be achieved, as expected. Additionally, the impact of pointing errors with nonzero boresight on the total ABER performance was highlighted. In fact, the depicted results revealed significant ABER degradations when the ξ_2 parameter ranged from 0.87 to 0.96; i.e., as nonzero boresight pointing errors were getting weaker. It also became evident that the spatial-diversity technique could significantly alleviate the negative side effects of NZB misalignments. Indeed, for the same amount of pointing mismatch, we could observe significantly reduced corresponding ABER values as the diversity order was higher; e.g., as M becameequal to 3 instead of 2; i.e., by utilizing one more photodetector at the receiver's side. Nevertheless, the significant availability enhancements that stemmed from diversity-method employment were realized at the expense of a higher degree of system complexity, along with lower achievable data rates. Thus, it was not wise to further increase the diversity order of the proposed MRR TOW system.

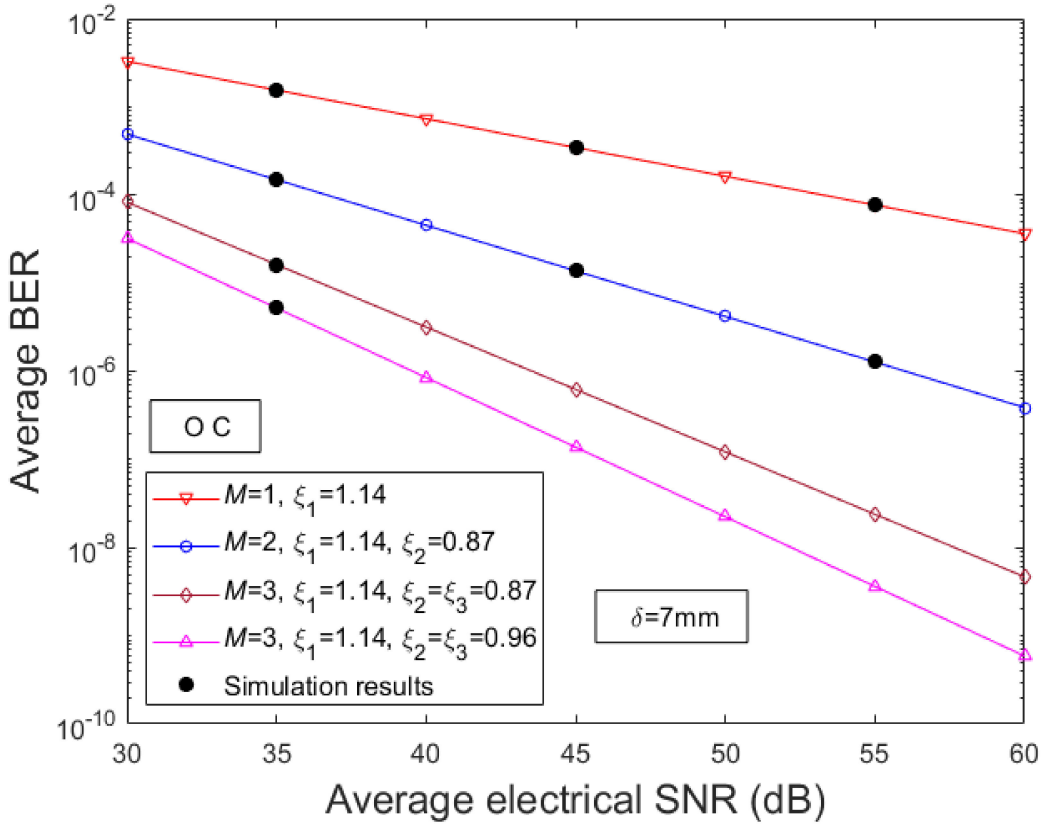

Figure 2. Average BER evolution over a wide range of electrical average SNR for various link configurations of $\delta_m = 7$ mm with spatial diversity and OC along withvarying generalized PE.

Figure 3 highlights the impact of skin thickness, which, according to Equation (6), is highly related to pointing-error strength, on the total ABER of SIMO MRR TOW links with OC. In this context, the only difference between the link configurations in Figures 2 and 3 was the transdermal link length, which was assumed to be extended by 1mm for each link. Therefore, although we assumed for both figures the same values for the parameter set $\left(\mu_{x,m}/r_m,\ \mu_{y,m}/r_m,\ \sigma_{x,m}/r_m,\ \sigma_{y,m}/r_m\right)$, we eventually observed that the corresponding ξ_1, ξ_2 and ξ_3 hadbeen increased due to Equation (6). The latter translated into a weaker amount of both zero and NZB pointing mismatch, and led to an enhanced ABER performance. For typical skin thicknesses, this behavior was consistent with findings in [11], until skin-induced attenuation became the dominant effect. It should be also noted that as is the case in Figure 2, the impact of NZB was stronger than the impact of zero-boresight pointing errors. This is because the laser could be strictly aligned with only one receiver aperture (in the case of zero boresight). The unavoidable geometric distance between receiver apertures

caused the additional boresight pointing-error component, which aggravated the total pointing errors' negative side effects.

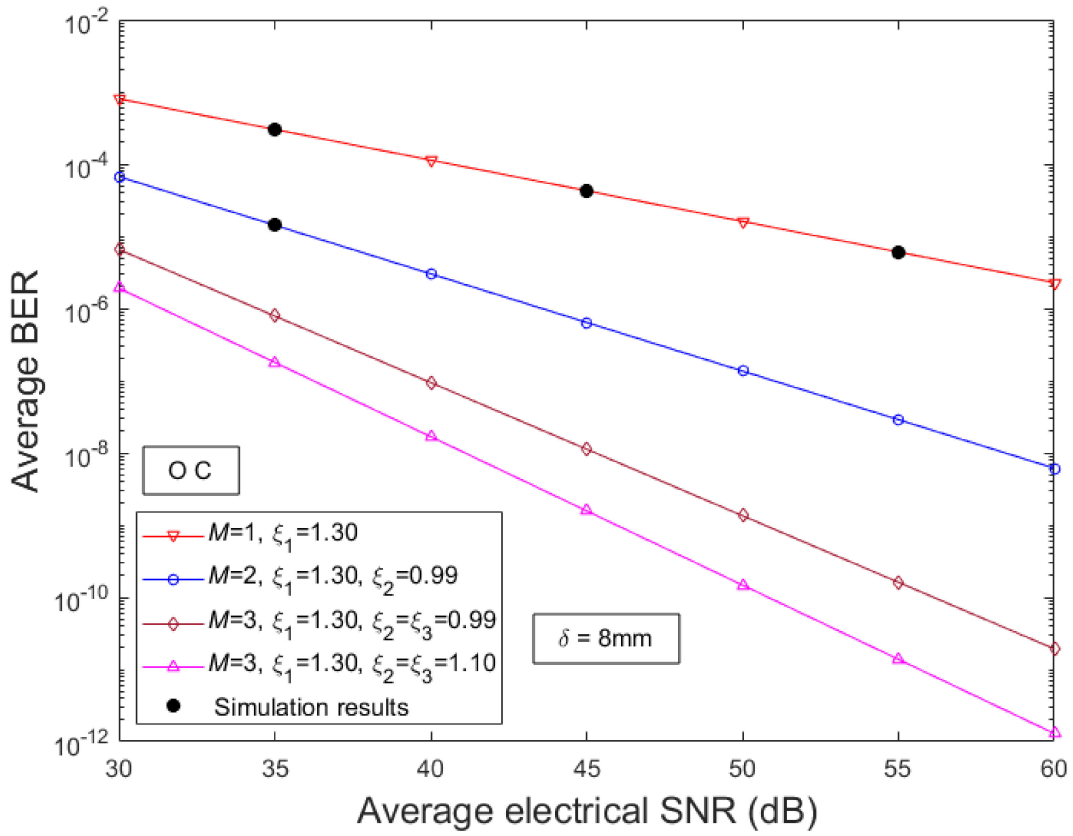

Figure 3. Average BER evolution over a wide range of electrical average SNR for various link configurations of $\delta_m = 8$ mm with spatial diversity and OC along withvarying generalized PE.

Figure 4 illustrates whether the examined average electrical SNR regime, which ensures an adequate ABER performance, could be implemented or not due to the transdermal pathloss and other power limitations. Specifically, the most power-consumption-demanding biomedical applications with IMDs require a signal PSD from 1 μW/MHz to 20 μW/MHz. Within this desirable signal PSD regime, the illustrated results revealed that the attainable average electrical SNR values assumed adequate levels in response to pointing errors with NZB, transdermal pathloss, transmission power requirements and ABER performance requirements. It also became evident that by increasing the transmission power, higher average SNR values were achieved that could lead to more significant mitigations of the joint impact of skin-induced attenuation along with NZB pointing-error effects, as shown in Figures 2 and 3. Alternatively, in an attempt to increase the received signal level so as to address this joint impact, we could use a large photodetector aperture(s). Nevertheless, larger photodiodes lead to limited bandwidth [23], which results in lower data rates. Thus, we tried to keep a balance between power consumption, the photodiode's size aperture and depth of penetration of light through the skin.

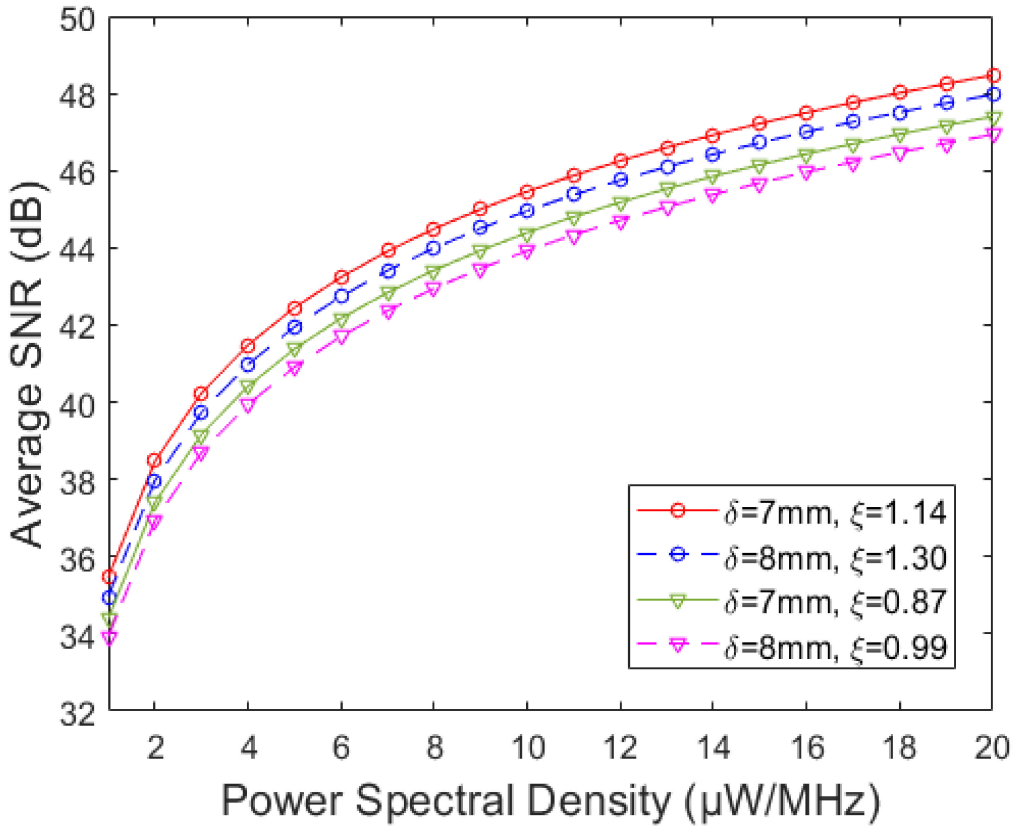

Figure 4. Average SNR evolution over a wide range of power spectral density of the transmitted signal for various generalized pointing errors strength and skin thicknesses.

For a real human body, its specific characteristics, including different skin conditions such as thickness, smoothness, tissue particularities, age, race, sweat, body temperature and anatomy of the intended user, should be taken into consideration. In any case, however, human skin is partially transparent to light at wavelengths ranging from 600 to 1300 nm, while also only 10% to 30% of incident optical power can be transmitted through skin of typical thickness due to skin attenuation [8]. Having fixed the operational wavelength at 1100nm and having used Equation (4) to evaluate the human skin-induced attenuation coefficient, which presented an accuracy higher than 99.7% for this wavelength region [19], it became evident that even in the worst scenario, the results obtained from a real human body would be slightly different. Moreover, although human body temperature (which usually ranges between 36 and 37 °C) where the MRR is located is different than the out-of-body typical room temperature (25 °C), the response of typical MRRs shifts slightly by such temperature and/or wavelength changes. Furthermore, although larger depths in the tissue require larger MRRs size, the dimensions of typical MRRs allow their establishment inside human skin for common medical applications [4]. Additionally, the proposed model seemed to be valid for weak to strong generalized pointing errors. In fact, the investigated pointing-error parameter values covered a wide range of misalignments caused by patients' and/or human organs' realistic movements. In view of the above, we can remark that without loss of generality, the proposed model was in a good agreement with human skin characteristics.

4. Discussion

In this work, a performance analysis in terms of ABER was first presented for SISO and SIMO MMR TOW links with spatial diversity and OC technique, under the presence of NZB stochastic pointing errors. Additionally, considering both transdermal pathloss together with the strict power requirements of many biomedical applications with IMDs, the average

attainable electrical SNR was evaluated. In this context, novel analytical average SNR and ABER expressions were derived. By utilizing them, proper representative analytical results were presented and verified further through simulations over a wide average electrical SNR range, for several MRR TOW link configurations with multiple receivers, typical skin thicknesses along with varying stochastic zero boresight and NZB pointing errors. Our findings demonstrated encouraging attainable ABER values, especially when NZB boresight pointing errors were getting weaker and multiple photodetectors were employed. Additionally, apart from increasing the number of effective TOW backward links through spatial diversity, it is also crucial to bear in mind that skin thickness influences not only transdermal pathloss, but also zero-boresight and/or nonzero-boresight pointing-error effects. Furthermore, it is wise to select the operational optical wavelength within the medical optical window, more precisely around 1100 nm, in order to minimize skin-induced attenuation detrimental effects. The latter becomes even more critical for the design of MRR TOW systems, since in such cases, the light beam traverses the skin channel twice to reach the receiver's side. Consequently, it is noteworthy and also encouraging in the design of a TOW MRR system that even in the worst-case scenario investigated—including the stronger generalized stochastic pointing errors, the larger transdermal propagation distance, and the lowest PSD for the optical signal—having selected 1100nm as the operational wavelength for each transdermal linkand having selected also appropriate skin thicknesses to place the retromodulator, we achieved adequate average electrical SNR, which can offer, as demonstrated, significant ABER enhancements, especially when spatial diversity is properly utilized.

5. Conclusions

Nowadays, TOW systems area viable effective alternative to common wireless communication modalities used for transdermal communication that are based on radio frequency (RF), acoustic waves, conduction or electrical induction. Still, improving communication with medical-implant devices remains an important topic of research that requires particular attention to critical TOW link parameters such as tissue thickness, optical operational wavelengths, power consumption for the medical implanted device, and transmitter and receiver aperture size, as well as MRR link particularities when utilized. Making the appropriate trade-offs and by incorporating novel performance-effective techniques, e.g., in terms of diversity, we may move toward to the design of more sophisticated, reliable and energy-effective TOW links. Thus, through the proposed architecture, we have achieved the design of a SIMO MMR TOW system with enhanced ABER performance and availability.

However, considering the detrimental impact of pointing errors with nonzero boresight, a major drawback of the proposed TOW architecture is that a tracking system on the out-of-body unit could be required to further upgrade the total TOW performance and availability, which, however, increases the system's complexity. In this respect, an out-of-body, obstacle-free environment between transmitted and reflected paths should be ensured. Furthermore, for MRR TOW link realizations, it is required that there should bean adequate in-body space for modulated retroreflector establishment, which in turn should be sufficiently compact in size for use in medical implants inside the body.

Author Contributions: Conceptualization, G.K.V., H.E.N. and K.A.; methodology, G.K.V., H.E.N. and K.A.; software, G.K.V.; validation, G.K.V., H.E.N., K.A., F.J., M.N. and K.K.M.R.; investigation, G.K.V., H.E.N., K.A., F.J., M.N. and K.K.M.R.; resources, G.K.V., H.E.N., K.A., F.J., M.N. and K.K.M.R.; writing—original draft preparation, G.K.V.; writing—review and editing, G.K.V. and H.E.N.; supervision, G.K.V., H.E.N. and K.A.; funding acquisition, G.K.V., H.E.N. and K.A. All authors have read and agreed to the published version of the manuscript.

Funding: This research was funded by Ajman University under grant number 2020-IRG-ENIT-02.

Institutional Review Board Statement: Not applicable.

Informed Consent Statement: Not applicable.

Data Availability Statement: Not applicable.

Conflicts of Interest: The authors declare no conflict of interest.

References

1. Gil, Y.; Rotter, N.; Arnon, S. Feasibility of retroreflective transdermal optical wireless communication. *Appl. Opt.* **2012**, *51*, 4232–4239. [CrossRef] [PubMed]
2. Guillory, K.S.; Misener, A.K.; Pungor, A. Hybrid RF/IR transcutaneous telemetry for power and high-bandwidth data. In Proceedings of the 26th Annual International Conference of the IEEE Engineering in Medicine and Biology Society, San Francisco, CA, USA, 1–5 September 2004; IEEE: Piscataway, NJ, USA, 2004; pp. 4338–4340.
3. Abualhoul, M.Y.; Svenmarker, P.; Wang, Q.; Andersson, J.Y.; Johansson, A.J. Free space optical link for biomedical applications. In Proceedings of the 2012 Annual International Conference of the IEEE Engineering in Medicine and Biology Society, San Diego, CA, USA, 28 August–1 September 2012; IEEE: Piscataway, NJ, USA, 2012; pp. 1667–1670.
4. Varotsos, G.K.; Nistazakis, H.E.; Aidinis, K.; Jaber, F.; Rahman, K.K.M.; Tsigopoulos, A.D.; Christofilakis, V. Average BER Estimation of Retroreflective Transdermal Optical Wireless Links with Diversity, Attenuation and Spatial Jitter. In Proceedings of the 2020 International Conference on Modern Circuits and Systems Technologies (MOCAST), Bremen, Germany, 7–9 September 2020; IEEE: Piscataway, NJ, USA, 2020; pp. 1–4.
5. Varotsos, G.K.; Nistazakis, H.E.; Aidinis, K.; Jaber, F.; Rahman, K.K.M. Transdermal subcarrier L-PSK or DBPSK optical wireless links with time diversity, skin attenuation and spatial jitter. *J. Modern Opt.* **2020**, *67*, 14. [CrossRef]
6. Varotsos, G.K.; Nistazakis, H.E.; Aidinis, K.; Jaber, F.; Rahman, K.K.M. Signal Intensity Estimation in Transdermal Optical Wireless Links with Stochastic Pointing Errors Effect. *Technologies* **2020**, *8*, 60. [CrossRef]
7. Parmentier, S.; Fontaine, R.; Roy, Y. Laser diode used in 16 Mb/s, 10 mW optical transcutaneous telemetry system. In Proceedings of the Biomedical Circuits and Systems Conference, BioCAS, Baltimore, MD, USA, 20–22 November 2008; IEEE: Piscataway, NJ, USA, 2008; pp. 377–380.
8. Liu, T.; Bihr, U.; Anis, S.M.; Ortmanns, M. Optical transcutaneous link for low power, high data rate telemetry. In Proceedings of the 2012 Annual International Conference of the IEEE Engineering in Medicine and Biology Society (EMBC), San Diego, CA, USA, 28 August–1 September 2012; IEEE: Piscataway, NJ, USA, 2012; pp. 3535–3538.
9. Liu, T.; Anders, J.; Ortmanns, M. System level model for transcutaneous optical telemetric link. In Proceedings of the 2013 IEEE International Symposium on Circuits and Systems (ISCAS), Beijing, China, 19–23 May 2013; IEEE: Piscataway, NJ, USA, 2013; pp. 865–868.
10. Liu, T.; Bihr, U.; Becker, J.; Anders, J.; Ortmanns, M. In vivo verification of a 100 Mbps transcutaneous optical telemetric link. In Proceedings of the Biomedical Circuits and Systems Conference (BioCAS), Lausanne, Switzerland, 22–24 October 2014; IEEE: Piscataway, NJ, USA, 2014; pp. 580–583.
11. Trevlakis, S.E.; Boulogeorgos, A.A.A.; Sofotasios, P.C.; Muhaidat, S.; Karagiannidis, G.K. Optical wireless cochlear implants. *Biomed. Opt. Express* **2019**, *10*, 707–730. [CrossRef] [PubMed]
12. Varotsos, G.K.; Nistazakis, H.E.; Aidinis, K.; Jaber, F.; Rahman, K.K. Transdermal Optical Wireless Links with Multiple Receivers in the Presence of Skin-Induced Attenuation and Pointing Errors. *Computation* **2019**, *7*, 33. [CrossRef]
13. Ackermann, D.M.; Smith, B.; Kilgore, K.L.; Peckham, P.H. Design of a high speed transcutaneous optical telemetry link. In Proceedings of the 2006 International Conference of the IEEE Engineering in Medicine and Biology Society, New York, NY, USA, 30 August–3 September 2006; IEEE: Piscataway, NJ, USA, 2006; pp. 2932–2935.
14. Abita, J.L.; Schneider, W. *Transdermal Optical Communications*; John Hopkins APL Tech: Laurel, MD, USA, 2004; Volume 25, pp. 261–268.
15. Ackermann, D.M.; Smith, B.; Wang, X.F.; Kilgore, K.L.; Peckham, P.H. Designing the optical interface of a transcutaneous optical telemetry link. *IEEE Trans. Biomed. Eng.* **2008**, *55*, 1365–1373. [CrossRef] [PubMed]
16. Ritter, R.; Handwerker, J.; Liu, T.; Ortmanns, M. Telemetry for implantable medical devices: Part 1-media properties and standards. *IEEE Solid-State Circuits Mag.* **2014**, *6*, 47–51. [CrossRef]
17. Varotsos, G.K.; Nistazakis, H.E.; Tombras, G.S.; Aidinis, K.; Jaber, F.; Rahman, M. On the use of diversity in transdermal optical wireless links with nonzero boresight pointing errors for outage performance estimation. In Proceedings of the 2019 International Conference on Modern Circuits and Systems Technologies (MOCAST), Thessaloniki, Greece, 7–9 May 2019; IEEE: Piscataway, NJ, USA, 2019; pp. 1–4.
18. Varotsos, G.K.; Nistazakis, H.E.; Aidinis, K.; Roumelas, G.D.; Jaber, F.; Rahman, K.K.M. Modulated Retro-Reflector Transdermal Optical Wireless Communication Systems with Wavelength Diversity over Skin-Induced Attenuation and Pointing Errors. In Proceedings of the 2020 IEE International Symposium on Signal Processing and Information Technology (ISSPIT), Ajman, United Arab Emirates, 10–12 December 2019; IEEE: Piscataway, NJ, USA, 2019; pp. 1–5.
19. Trevlakis, S.; Boulogeorgos, A.A.; Karagiannidis, G. Signal Quality Assessment for Transdermal Optical Wireless Communications under Pointing Errors. *Technologies* **2018**, *6*, 109. [CrossRef]
20. Varotsos, G.K.; Nistazakis, H.E.; Petkovic, M.I.; Djordjevic, G.T.; Tombras, G.S. SIMO Optical Wireless Links with Nonzero Boresight Pointing Errors over M modeled Turbulence Channels. *Elsevier Opt. Commun.* **2017**, *403*, 391–400. [CrossRef]
21. Varotsos, G.K.; Nistazakis, H.E.; Gappmair, W.; Sandalidis, H.G.; Tombras, G.S. SIMO subcarrier PSK FSO links with phase noise and non-zero boresight pointing errors over turbulence channels. *IET Commun.* **2019**, *13*, 831–836. [CrossRef]

22. Navidpour, S.M.; Uysal, M.; Kavehrad, M. BER performanceof free-space optical transmission with spatial diversity. *IEEE Trans. Wirel. Commun* **2007**, *6*, 2813–2819.
23. Ghassemlooy, Z.; Arnon, S.; Uysal, M.; Xu, Z.; Cheng, J. Emerging optical wireless communications-advances and challenges. *IEEE J. Sel. Areas Commun.* **2015**, *33*, 1738–1749. [CrossRef]
24. Trevlakis, S.E.; Boulogeorgos, A.A.A.; Karagiannidis, G.K. On the impact of misalignment fading in transdermal optical wireless communications. In Proceedings of the 7th International Conference on Modern Circuits and Systems Technologies (MOCAST), Thessaloniki, Greece, 7–9 May 2018; IEEE: Piscataway, NJ, USA, 2018; pp. 1–4.
25. Trevlakis, S.E.; Boulogeorgos, A.A.A.; Karagiannidis, G.K. Outage Performance of Transdermal Optical Wireless Links in the Presence of Pointing Errors. In Proceedings of the 2018 IEEE 19th International Workshop on Signal Processing Advances in Wireless Communications (SPAWC), Kalamata, Greece, 25–28 June 2018; IEEE: Piscataway, NJ, USA, 2018; pp. 1–5.
26. Li, X.; Zhao, X.; Zhang, P.; Yang, W.; Wang, T.; Jiang, H. Probability density function of turbulence fading in MRR free space optical link and its applications in MRR free space optical communications. *IET Commun.* **2017**, *11*, 2476–2481. [CrossRef]
27. Farid, A.A.; Hranilovic, S. Outage capacity optimization for free space optical links with pointing errors. *IEEE/OSA J. Lightwave Technol.* **2007**, *25*, 1702–1710. [CrossRef]
28. Yang, F.; Cheng, J.; Tsiftsis, T.A. Free-space optical communication with nonzero boresight pointing errors. *IEEE Trans. Commun.* **2014**, *62*, 713–725. [CrossRef]
29. Boluda-Ruiz, R.; Garcia-Zambrana, A.; Castillo-Vazquez, B.; Castillo-Vazquez, C. Impact of nonzeroboresight pointing error on ergodic capacity of MIMO FSO communication systems. *Opt. Express* **2016**, *24*, 3513–3534. [CrossRef] [PubMed]
30. Boluda-Ruiz, R.; García-Zambrana, A.; Castillo-Vazquez, C.; Castillo-Vazquez, B. Novel approximation of misalignment fading modeled by Beckmann distribution on free-space optical links. *Opt. Express* **2016**, *24*, 22635–22649. [CrossRef] [PubMed]
31. Gradshteyn, I.S.; Ryzhik, I.M. *Table of Integrals, Series, and Products*, 6th ed.; Academic Press: New York, NY, USA, 2000.
32. Beckmann, P.; Spizzichino, A. *The Scattering of Electromagnetic Waves from Rough Surfaces*; Artech House: Norwood, MA, USA, 1987.
33. Helstrom, C.W. *Probability and Stochastic Processes for Engineers*; Macmillan Coll Division: Stuttgart, Germany, 1991.
34. The Wolfarm Functions Site. 2008. Available online: https://functions.wolfram.com/ (accessed on 30 November 2020).
35. Chiani, M.; Dardari, D.; Simon, M.K. New exponential bounds and approximations for the computation of error probability in fading channels. *Trans. Wireless Commun.* **2003**, *2*, 840–845. [CrossRef]
36. Alouini, M.-S.; Simon, M.K. An MGF-based performance analysis of generalized selection combining over Rayleigh fading channels. *IEEE Trans. Commun.* **2000**, *48*, 401–415. [CrossRef]
37. Maxim Integrated Products. 155 Mbps Low-Noise Transimpedance Amplifier. Available online: http://pdf.datasheetcatalog.com/datasheets2/44/444242_1.pdf (accessed on 30 November 2020).